AFRL-RX-WP-JA-2016-0301

LONG DISTANCE ENHANCEMENT OF NONLINEAR OPTICAL PROPERTIES USING LOW CONCENTRATION OF PLASMONIC NANO-STRUCTURES IN DYE DOPED MONOLITHIC SOL–GEL MATERIALS (POSTPRINT)

D. Chateau, A. Liotta, F. Lerouge, F. Chaput, and S. Parola
Université de Lyon

H. Lundén and C. Lopes
Swedish Defense Research Agency

D. Krein and T. Cooper
AFRL/RX

A.A.G. El-Amay and M. Lindgren
Norwegian University of Science and Technology

23 September 2015
Interim Report

(STINFO COPY)
AIR FORCE RESEARCH LABORATORY
MATERIALS AND MANUFACTURING DIRECTORATE
WRIGHT-PATTERSON AIR FORCE BASE, OH 45433-7750
AIR FORCE MATERIEL COMMAND
UNITED STATES AIR FORCE

REPORT DOCUMENTATION PAGE

Form Approved
OMB No. 0704-0188

1. REPORT DATE *(DD-MM-YY)*	2. REPORT TYPE	3. DATES COVERED *(From - To)*
23 September 2015	Interim	31 January 2014 – 23 August 2015

4. TITLE AND SUBTITLE

LONG DISTANCE ENHANCEMENT OF NONLINEAR OPTICAL PROPERTIES USING LOW CONCENTRATION OF PLASMONIC NANO-STRUCTURES IN DYE DOPED MONOLITHIC SOL–GEL MATERIALS (POSTPRINT)

5a. CONTRACT NUMBER
FA8650-09-D-5434-0026

5b. GRANT NUMBER

5c. PROGRAM ELEMENT NUMBER
62102F

6. AUTHOR(S)

1) D. Chateau, A. Liotta, F. Lerouge, F. Chaput, and S. Parola – Universite de Lyon

2 H. Lundén and C. Lopes – Swedish Defense Research Agency

(continued on page 2)

5d. PROJECT NUMBER
4348

5e. TASK NUMBER 0026

5f. WORK UNIT NUMBER
X0V5

7. PERFORMING ORGANIZATION NAME(S) AND ADDRESS(ES)

1) Université de Lyon
CNRS UMR5182, Lyon 69364
France

2) Swedish Defence Research Agency (FOI), Linköping
SE-581 11, Sweden

(continued on page 2)

8. PERFORMING ORGANIZATION REPORT NUMBER

9. SPONSORING/MONITORING AGENCY NAME(S) AND ADDRESS(ES)

Air Force Research Laboratory
Materials and Manufacturing Directorate
Wright-Patterson Air Force Base, OH 45433-7750
Air Force Materiel Command
United States Air Force

10. SPONSORING/MONITORING AGENCY ACRONYM(S)
AFRL/RXAP

11. SPONSORING/MONITORING AGENCY REPORT NUMBER(S)
AFRL-RX-WP-JA-2016-0301

12. DISTRIBUTION/AVAILABILITY STATEMENT
Distribution Statement A. Approved for public release: distribution unlimited.

13. SUPPLEMENTARY NOTES
PA Case Number: 88ABW-2015-4357; Clearance Date: 23 Sep 2015. This document contains color. Journal article published in Advanced Functional Materials, Vol. 26, No.33, 31 May 2016.
The final publication is available at www.afm-journal.de DOI: 10.1002/adfm.201601646

14. ABSTRACT *(Maximum 200 words)*

Monolithic sol–gel silica composites incorporating platinum-based chromophores and various types of gold nanoparticles (AuNPs) are prepared and polished to high optical quality. Their photophysical properties are investigated. The glass materials show well-defined localized surface plasmon resonance (SPR) absorbance from the visible to NIR. No redshifts of the AuNP plasmon absorption peaks due to the increase in nanoparticle doping concentration are observed in the glasses, proving that no or very small SPR coupling effects occur between the AuNPs. At 600 nm excitation, but not at 532 nm, the AuNPs improve the nonlinear absorption performance of glasses codoped with 50 × 10−3 m of a Pt-acetylide chromophore. The glasses doped with lower concentrations of AuNPs (2–5 μm average distance) and 50 × 10−3 m in chromophore, show a marked improvement in nonlinear absorption, with no or only small improvement for the more highly AuNP doped glasses. This study shows the importance of excitation wavelength and nanoparticle concentration for composite systems employing AuNPs to improve two-photon absorption of chromophores.

15. SUBJECT TERMS
Monolithic sol–gel silica composites; platinum-based chromophores; surface plasmon resonance (SPR); gold nanoparticles

16. SECURITY CLASSIFICATION OF:			17. LIMITATION OF ABSTRACT:	18. NUMBER OF PAGES	19a. NAME OF RESPONSIBLE PERSON (Monitor)
a. REPORT	b. ABSTRACT	c. THIS PAGE			Timothy White
Unclassified	Unclassified	Unclassified	SAR	13	19b. TELEPHONE NUMBER *(Include Area Code)* (937) 255-9551

REPORT DOCUMENTATION PAGE Cont'd

6. AUTHOR(S)

3) D. Krein and T. Cooper - AFRL/RX

4) A.A.G. El-Amay and M. Lindgren - NUST

7. PERFORMING ORGANIZATION NAME(S) AND ADDRESS(ES)

3) AFRL/RX, Wright-Patterson AFB, OH 45433

4) Norwegian University of Science and Technology
Trondheim NO-7491 , Norway

Long Distance Enhancement of Nonlinear Optical Properties Using Low Concentration of Plasmonic Nanostructures in Dye Doped Monolithic Sol–Gel Materials

Denis Chateau, Adrien Liotta, Hampus Lundén, Frederic Lerouge, Frederic Chaput, Douglas Krein, Thomas Cooper, Cesar Lopes, Ali A. G. El-Amay, Mikael Lindgren, and Stephane Parola**

Monolithic sol–gel silica composites incorporating platinum-based chromophores and various types of gold nanoparticles (AuNPs) are prepared and polished to high optical quality. Their photophysical properties are investigated. The glass materials show well-defined localized surface plasmon resonance (SPR) absorbance from the visible to NIR. No redshifts of the AuNP plasmon absorption peaks due to the increase in nanoparticle doping concentration are observed in the glasses, proving that no or very small SPR coupling effects occur between the AuNPs. At 600 nm excitation, but not at 532 nm, the AuNPs improve the nonlinear absorption performance of glasses codoped with 50×10^{-3} M of a Pt-acetylide chromophore. The glasses doped with lower concentrations of AuNPs (2–5 µm average distance) and 50×10^{-3} M in chromophore, show a marked improvement in nonlinear absorption, with no or only small improvement for the more highly AuNP doped glasses. This study shows the importance of excitation wavelength and nanoparticle concentration for composite systems employing AuNPs to improve two-photon absorption of chromophores.

1. Introduction

Synergy between nanoparticles and chromophores has become a feasible way to control and modify optical effects.[1–15] The strategies used have been either to bond or adsorb the chromophore directly to the nanoparticle for intramolecular-nanoparticle cooperation or in a nonbonding fashion for intermolecular-nanoparticle cooperation. Gold nanoparticles (AuNPs) have attracted much attention for optical enhancement applications as AuNPs can be prepared in various shapes, are chemically stable, and the surface plasmon resonance (SPR) can be controlled.[2,5,9,12,16–20] The observed optical effects have their origin in the electric field intensity enhancement created by the SPR absorption.[1,4,21,22] In close contact the coupling between the nanoparticle and the chromophore gives rise to a plasmon shift. This plasmon shift disappears at longer separations between the nanoparticle and the chromophore.[15] Whether in close contact or at a distance, nanoparticles have proven to be able to improve the efficiency in applications such as solar cells,[23–27] photorefractivity,[28] upconversion,[29] Freedericksz transition,[30] spin crossover,[31] nonlinear absorption (NLA),[32–36] and surface-enhanced Raman Scattering.[9]

In this paper we report the synergetic effect between a platinum acetylide-based chromophore and AuNPs for nonlinear optical applications. The organometallic platinum acetylides are known to show broadband nonlinear optical absorption, with a wavelength dependence of the nonlinear optical mechanism; singlet ground state one-photon absorption with fast intersystem crossing (ISC) to the triplet state dominates <500 nm, direct ground state singlet to triplet absorption in the range

Dr. D. Chateau, A. Liotta, Dr. F. Lerouge, Dr. F. Chaput, Prof. S. Parola
Laboratoire de Chimie
Université de Lyon
Ecole Normale Supérieure de Lyon
Université Claude Bernard Lyon 1
CNRS UMR5182, Lyon 69364, France
E-mail: stephane.parola@univ-lyon1.fr

H. Lundén, Dr. C. Lopes
Electrooptical Systems
Swedish Defence Research Agency (FOI)
Linköping SE-581 11, Sweden
E-mail: hampus.lunden@foi.se

Dr. D. Krein, Dr. T. Cooper
Air Force Research Laboratory
Dayton, OH 45433, USA

Dr. A. A. G. El-Amay, Prof. M. Lindgren
Department on Physics
Norwegian University of Science and Technology
Trondheim NO-7491, Norway

DOI: 10.1002/adfm.201601646

≈500–570 nm,[37–39] and two-photon absorption (2PA) with fast ISC to the triplet state in the range ≈540–700 nm.[40,41] Earlier reports, on liquid mixtures and thin films, suggested that the interaction between an organic chromophore and AuNPs leads to an enhancement of two- and three-photon absorption.[11,13,42] In such chromophore–nanoparticle systems, it is now well established that the control of the chromophore-to-nanoparticle distance and orientation of the chromophore's dipole at the surface of the nanoparticles is crucial to achieve the proper coupling between the plasmon resonance and the chromophore (in particular the relaxation properties of the photoactivated excited state) but this remains difficult to control. The chromophores need to be located in a suitable distance ranging from about 10 to 20 nm to achieve optimum emission enhancement according to theoretical predictions.[43,44] At shorter distances the emission appears to be systematically quenched due to energy transfer to the nanoparticle metal surface. At longer distances, no effect is commonly detected. The chromophore–nanoparticle interdistance control has been successfully achieved through different strategies applied on the nanoparticles; e.g., by the use of polyelectrolyte or polymer spacers, core-shell structures, or multilayer thin films. The possibility to observe strong enhancement of excited state populations and its kinetics in high-spin organometallic systems with AuNPs still remains an important challenge. In this work, the nonlinear absorption is enhanced for a Pt-acetylide chromophore known to have triplet states sensitive to the presence of oxygen.[45,46]

The preparation of monolithic bulk composite hybrid optical materials, with codispersion of both chromophores and plasmonic nanostructures in a homogeneous way, has not yet been reported. We propose a sol–gel approach to prepare such optical composites. The idea is to use the SPR effect to induce local field enhancement as well as interplay with excited states of the codoped chromophores in a monolithic composite. Different sizes and geometrical shapes, spherical and bipyramidal, and concentrations of the nanoparticles, were used in order to investigate the effect on the Pt-acetylide chromophore. Bipyramidal nanoparticles were chosen due to their versatility regarding different SPR wavelengths and the high field intensities near their tips.[20] Incorporation of efficient nonlinear dyes into a solid matrix at high concentration is a real challenge. This has been achieved through the sol–gel process, which allows preparation of high-optical quality xerogels[37,47–50] with controlled structure and efficient dispersion of thermosensitive chromophores in high concentrations.[37,49,50] Similarly, it was possible to incorporate metal nanoparticles in monolithic sol–gel matrices for nonlinear optical purposes.[51] We report here the use of SPR materials to enhance the nonlinear optical properties, and in particular the multiphoton absorption processes by codoping sol–gel matrices with a Pt-acetylide chromophore and AuNPs. The chromophore used allows for highly doped sol–gel glasses easily polished to an excellent optical quality.[37] Moreover, the NLA investigations illustrate the significant contribution of the SPR on the two-photon absorption efficiency, even at low concentrations of the nanoparticles. To our knowledge, this is the first reported enhancement of nonlinear absorption of a chromophore in a bulk material by field enhancement of its two-photon absorption by nanoparticles. This opens up the possibility to enhance the performance of a wide class of nonlinear photonic devices employing two photon absorption. Our findings also illustrate the importance of nanoparticle concentration for optimum performance. This is of interest for a wide range of applications where nanoparticles are used to enhance nonlinear absorption by field enhancement.

2. Results and Discussion

Materials with high concentration of platinum chromophores were previously reported showing the important potential of the sol–gel method to prepare efficient NLA materials.[37,50] Moreover, we were able to prepare gold nanoparticle doped sol–gel monolithic composites, which showed interesting self-orientation structures in the case of anisotropic particles. Those monolithic glasses had, though, limited nonlinear scattering efficiency at 600 nm.[51]

2.1. Synthesis and Structural Characterization of the Materials

Two types of gold spheres (diameters of 23 and 45 nm with absorption maximum at 523 and 532 nm, respectively) and three types of anisotropic bipyramidal AuNPs were prepared exhibiting longitudinal plasmon resonance (LSPR) at 640, 700, and 770 nm, respectively (transmission electron microscopy (TEM)) images of the bipyramids are shown in **Figure 1**). Their detailed size parameters and compositions are given in **Table 1**. The chemical structure of the functional silicone used for their surface modification is shown in **Figure 2**. The monolithic materials were prepared using an adapted procedure from previously reported approach, allowing high concentration of the chromophores.[37,50–52] The structure of the model platinum-based chromophore **(1)** is shown in **Figure 3**. The materials presented here were prepared using the fast condensation sol–gel process and codoping with both chromophores and nanoparticles. The method, thus, allowed easy simultaneous codispersion of metal nanoparticles by adding the appropriate amount of silicone functionalized gold nanoparticles dispersed in tetrahydrofuran (THF) just before addition of the amine condensation catalyst aminopropyltetraethoxysilane (APTES).[37,49–51] The process gave glasses with high concentration (50×10^{-3} M) of the platinum chromophore and nanoparticles (three different concentrations for each nanoparticle with different LSPR) (**Figure 4**). The final solid materials were dried prior to optical polishing and measurements (**Figure 5**). They showed good dispersion of the dopants, high homogeneity, and optical quality.

2.2. Optical Characterizations

2.2.1. Spectroscopic Investigation of Dye and NPs in THF

In order to obtain the basic photophysical behavior of the system of the platinum chromophore **(1)** together with AuNPs, the properties were first examined in THF solutions. The absorption spectra of a series of samples are shown in **Figure 6**, left. Spherical AuNPs with a diameter of 45 nm were used, giving

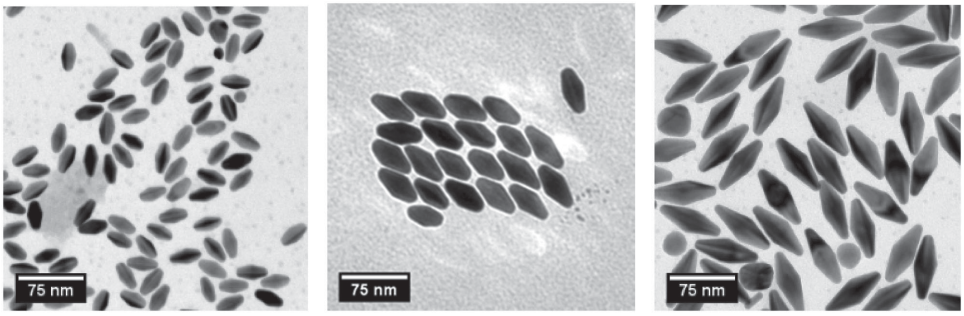

Figure 1. TEM images of the respective nanoparticles: gold bipyramids longitudinal surface plasmon resonance (LSPR) at 640, 700, and 770 nm (from left to right).

rise to a plasmon absorption band around 550 nm. The absorption peak around 360 nm is from the well-known linear absorption band of **(1)**. The AuNP solutions have in addition a characteristic background due to Rayleigh scattering becoming stronger at shorter wavelengths. Three of the mixtures had identical concentration of **(1)** with the AuNP content varied. A fourth solution with only AuNP was made for reference. Excited state absorption (ESA) measurements were carried out using a 355 nm 5 ns long pulse as excitation and a white μs flash lamp was used to record the spectrum in a procedure reported previously.[38] The samples have been carefully flushed with argon gas to remove oxygen in order to avoid quenching of the triplet state.[38,45] The resulting ESA spectra are shown in Figure 6, right. As expected, for the sample containing only **(1)** in THF, the broad triplet-state absorption covers the whole visible range and peaks at ≈600 nm.[38] Interestingly the AuNPs solely dispersed in THF also exhibit a notable ESA response, basically as a broad almost constant background slightly sloping up toward the blue end of the spectrum. Thus, the dispersed AuNPs in THF show a decrease in transmission upon excitation at 355 nm compared to the nonexcited sample. For mixtures of AuNP and chromophore **(1)** there was a marked increase in overall ESA (**S1** and **S2** in Figure 6, right). THF containing only AuNPs shows an enhanced ESA (AuNPs in Figure 6, right). Also, when compensating by removing the contribution from the dispersion of only AuNP, there is an enhanced ESA from the triplet state of **(1)**. More details are revealed from the kinetics measurements (below).

The stability of the solutions were checked by remeasuring the optical absorption, shown as dashed lines in Figure 6, left. A clear blueshift of the plasmon resonance band is present, indicating that the AuNPs have been modified by the harsh treatment in the pump-and-probe measurements. The reported results must in such cases be treated with caution. The spectra shown in Figure 6, right are all from the very "first single shot".

In order to examine further properties of the triplet state, luminescence measurements were carried out. As is well known, removing oxygen from the solvent stabilizes the

Table 1. Different sample compositions for both spheres and bipyramids and the mean interparticle distances calculated in the monolithic materials (see Supporting Information for details).

AuNP type	Mean dimensions [nm]	[Au^0] [$\times 10^{-3}$ M]	[AuNP] [$\times 10^{-9}$ M]	Mean interparticle distance [μm]
Nanospheres	23 nm diameter	0.13	0.06	3.0
		0.25	0.13	2.3
		0.5	0.25	1.9
		1	0.5	1.5
	45 nm diameter	0.06	0.013	5.0
		0.13	0.026	4.0
		0.25	0.052	3.2
		0.5	0.1	2.6
Nanobipyramids	36 nm length	0.06	0.29	1.8
LSP@640 nm	16 nm diameter	0.13	0.58	1.4
	6 nm tip diameter	0.25	1.15	1.1
Nanobipyramids	50 nm length	0.06	0.12	2.4
LSP@700 nm	21 nm diameter	0.13	0.24	1.9
	8 nm tip diameter	0.25	0.48	1.5
Nanobipyramids	78 nm length	0.06	0.048	3.3
LSP@770 nm	28 nm diameter	0.13	0.097	2.6
	8 nm tip diameter	0.25	0.19	2.1

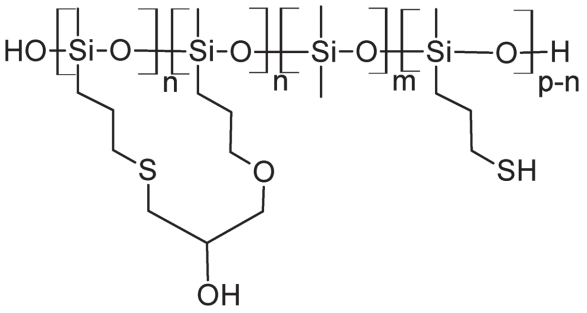

Figure 2. Structure of the functional silicone.

triplet states and thereby allowing for direct measurement of the chromophore's phosphorescence spectrum with emission maximum around 525 nm and its decay time.[37–39,45,46] A new series of samples with constant concentration of **(1)** and varying amounts of AuNP were prepared. (Their corresponding optical absorption and emission spectra upon excitation at 360 nm, are shown in the Supporting Information). As can be seen (Figure S8, right, Supporting Information) there was a drastic change in the emitted phosphorescence depending on the AuNP concentration. Since the plasmon band partially overlaps with the Pt-acetylide phosphorescence emission, decay-time measurements were carried out to assess the quenching by the AuNPs (**Figure 7**, left). The phosphorescence decay time of ≈50 µs for **(1)** in THF, concentration corresponding to OD 0.2, is drastically shortened to ≈30 µs by the addition of AuNPs to a concentration corresponding to OD 0.2 (sample **M3**, Figure S8, left, Supporting Information). Similar decay times were obtained when using the very same samples as used in the time-decay measurement of the phosphorescence (Figure 7, left) in the ESA set-up for kinetic studies. By monitoring the ESA at 600 nm (corresponding to the maximum triplet–triplet absorption of **(1)**) and collecting the transient optical absorption as an average of 5 excitation laser pulses, the decays as shown in Figure 7, right were obtained.

Just as in the case of the transient absorption spectra collected at 0 s time-delay, there is a marked increase of the triplet absorption in samples containing the AuNPs, however, only for concentrations corresponding to approximately OD 0.2. For higher concentrations of AuNPs the positive effect deteriorates (the recorded signal gets too noisy to allow analyses due to severe scattering).

Conclusively, the addition of small amounts of AuNPs to a moderately low concentration of **(1)** (more than approximately OD 0.2) gives a marked increase in ESA and quenching of phosphorescence with increased concentration of AuNPs. This is possible by enhancement of the singlet state formation, leading to increased triplet states formed by ISC for molecules of **(1)** in the vicinity of the AuNP. There is, however, a competing effect in terms of quenching of the triplet state by the plasmon resonance. Moreover, as the AuNPs concentration is further increased, the ESA deteriorates and a marked decrease in phosphorescence decay time occurs.

Figure 4. Materials prepared with 50×10^{-3} M chromophore **(1)** and gold nanoparticles with increasing concentration from bottom to top.

2.2.2. Optical Characterization of Glasses

As in the case of pure AuNPs doped methyl triethoxysilane (MTEOS) glasses reported previously,[51] the UV–vis transmission spectra of the AuNPs and chromophore **(1)** codoped MTEOS glasses showed well-defined plasmon absorption peaks, indicating a narrow size distribution of the AuNPs (representative spectra are shown in **Figure 8** and **Figure 9**, complementary spectra are shown in Figure S5, Supporting Information). The lack off (or marginal) redshifts with increasing AuNPs concentration indicate that, as with the AuNPs doped MTEOS glasses without chromophores,[51] the LSPR coupling effects from almost aggregated particles is negligible (see also Figure S5, Supporting Information).[53,54] Though, a blueshift of the plasmon wavelength compared to the nanoparticles in solution was found, similar to the glasses doped only with AuNPs.[51] The blueshift may be explainded by the change in the properties of the surrounding medium.

Nonlinear absorption measurements were performed at 532 and 600 nm. The measurements at 600 nm showed an improved performance for the samples doped with the lower concentrations of AuNPs. The improvements in nonlinear absorption with bipyramidal gold nanoparticles with a main LSP@640 nm are shown in **Figure 10**. (for the other shapes of AuNPs see the Supporting Information).

In order to investigate the relationship between AuNPs concentration and the nonlinear absorption performance, the mean output energy above input fluences of 10 J cm^{-2} was normalized to the linear transmission at 600 nm. A plot of the normalized output energy against the concentration of AuNPs showed an improved NLA performance for lower

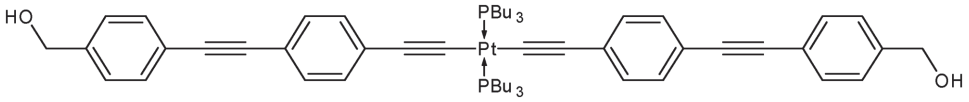

Figure 3. Structure of the platinum chromophore **(1)**.

Figure 5. Monoliths after optical polishing. The material with the highest concentration of AuBP (LSP@640 nm) is missing in the picture.

concentration of AuNPs (**Figure 11**). In other words, a large mean AuNP interparticle distance of several micrometers was found to be optimum for nonlinear absorption performance within the sample series. The pattern shown in Figure 11 is consistent for both spherical and bipyramidal AuNPs. Since similar platinum acetylide-based chromophores show 2PA in the range ≈540–700 nm,[40,41] the expected AuNPs 2PA enhancement[11,13,42] can explain the observed NLA improvement at this wavelength. Although, the pattern of improved NLA performance for lower concentrations of AuNPs was unexpected. Especially considering the low or nonexisting nonlinear absorption at 600 nm for MTEOS glasses doped solely with AuNPs.[51] Furthermore, the very low concentration of AuNPs required for nonlinear absorption enhancement is difficult to explain since there is a lack of strong LSPR shifts with different concentrations of AuNPs. To justify the suggested conclusion, a numerical population dynamics model was established. Hereby, the basic behavior can be explained in a qualitative manner as a balance between two-photon absorption enhancement and linear absorption before the focus point, details are outlined in section 2.2.3.

The nonlinear absorption performance at 532 nm with bipyramidal gold nanoparticles with LSP@640 nm is shown in **Figure 12** (for other shapes of AuNPs see the Supporting Information). A similar pattern, as for 600 nm (Figure 11), was not found for the 532 nm measurements (**Figure 13**). In the case of the 532 nm excitation wavelength measurements, a cutoff level was not observed. As a substitute, the mean output pulse energy of every input pulse with greater fluence than 150 J cm^{-2} was used. After normalization with the linear absorption at 532 nm, the lack of pattern in Figure 13 shows that the apparent improvement of nonlinear absorption from higher concentrations of AuNPs at 532 nm is predominantly from an increase in linear absorption. The lack of nonlinear absorption improvement for the 532 nm excitation would be expected since 532 nm is outside the 2PA band of similar Pt-chromophores.[40,41]

Compared to the nonlinear absorption at 532 nm for MTEOS glasses doped with only AuNPs,[51] the AuNP/chromophore **(1)** codoped MTEOS glasses show a lower nonlinear absorption performance. Considering that chromophore **(1)** glasses containing low concentrations of AuNPs show comparable performance to the MTEOS glasses doped solely with chromophore **(1)**, one can conclude that chromophore **(1)** affects the nonlinear scattering of AuNPs in MTEOS glass reported earlier.[51]

Luminescence spectra were taken with the solid glasses in reflection mode. The emission is dominated by fluorescence around 410 nm and the characteristic phosphorescence peak at 525 nm, well known for related systems (representative spectra are shown in Figure S7, Supporting Information). Lifetime measurements verified that the emission at 525 nm originated from phosphorescence with a decay time of ≈1 µs. Thus, the phosphorescence is seriously quenched by oxygen in glass pores as discussed previously.[37] Within experimental errors, there was no systematic difference in the emission spectra (Figure S7, Supporting Information) and phosphorescence decay times of the tested samples. Therefore, the mechanism behind the quenching of chromophore **(1)** by AuNPs in THF solution is not causing the lack of nonlinear absorption improvement for high concentration of AuNPs in glass.

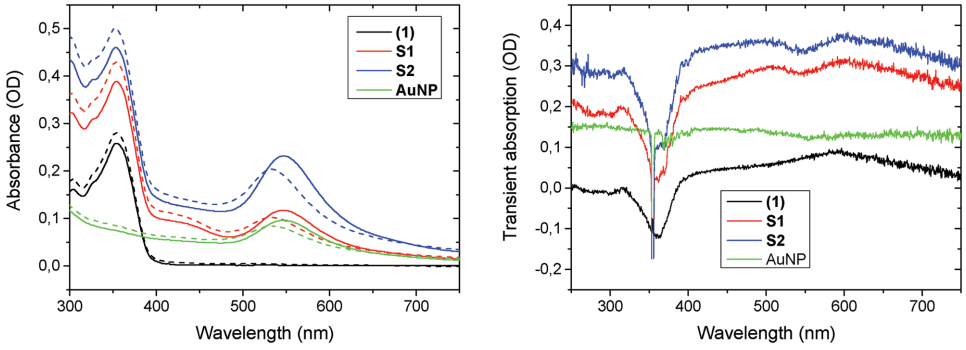

Figure 6. Left: Absorbance of samples for ESA series. (1) denotes solvent with compound **(1)** only. **S1** and **S2** had progressively increased AuNP concentration as indicated from the absorption spetra. AuNP denotes solvent with AuNP only (45 nm). Dashed lines are for measurements made after ESA measurements (see comment in text). Right: ESA of the solutes in left panel recorded at 0 s time-delay. The negative spike at 355 nm is residual from the pump-source.

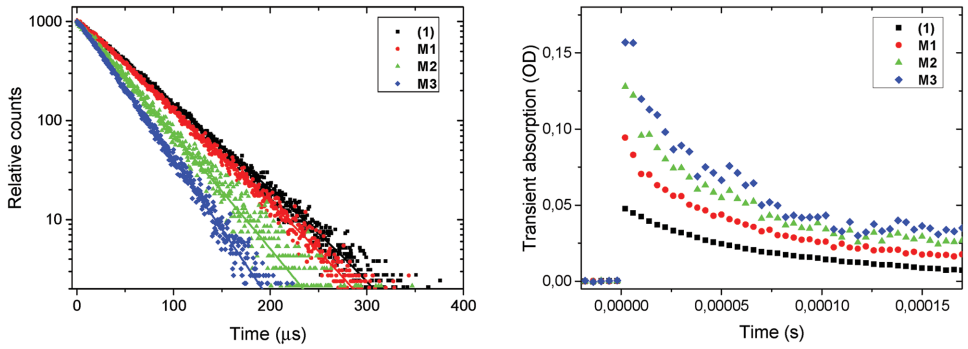

Figure 7. Left: Phosphorescence emission decays for excitation at 360 nm. Emission was monitored at 525 nm. Slits 2 nm (excitation) and 8 nm (emission). The concentration of **(1)** was chosen to give a peak absorbance of 0.2. **M1** additionally had 4×10^{-12} M of 45 nm diameter spherical AuNPs, **M2** 12×10^{-12} M, and **M3** 23×10^{-12} M (see Figure S8 in the Supporting Information for linear absorption spectra). The dashed lines are fits with decay times. **(1)** 51.2 +/–0.12 μs; **M1**: 47.1 +/–0.11 μs; **M2**: 38.0 +/–0.15 μs; **M3**: 30.8 +/–0.79 μs. Right: Kinetic decay of ESA at 600 nm for samples **(1), M1, M2**, and **M3** as in left panel and Figure S8 (Supporting Information). Each transient is an average of 5 pulses.

2.2.3. Population Model of the AuNPs/Chromophore **(1)** *Composite*

The nonlinear absorption enhancement and its dependence on AuNP concentration can be qualitatively explained by numerically modeling the population levels of chromophore **(1)** at a focal point. A similar method was used by Fischer et al.[55] to investigate the dynamics of populated levels from field enhancement of a light scattering AuNP. Herein, the method was applied to a two-photon process acting on a less complex population model at a single physical point in the sample. Also, no changes in transition probabilities were included in this model.

In the direction of maximum enhancement, the linear field enhancement factor (ratio of field intensities), η, can be expressed as

$$\eta = \left| 1 + 2\frac{a^3}{r^3}\frac{\varepsilon_1 - \varepsilon_m}{\varepsilon_1 + 2\varepsilon_m} \right|^2$$

where a is the nanoparticle radius, ε_1 the dielectric constants of the spherical gold nanoparticle, ε_m the dielectric constant of the surrounding medium and r the chromophore distance from the particle center.[56] The effective two-photon absorption coefficient can then be expressed as

$$\beta = \eta^2 \beta_0$$

where β_0 is the standard two-photon absorption coefficient defined by

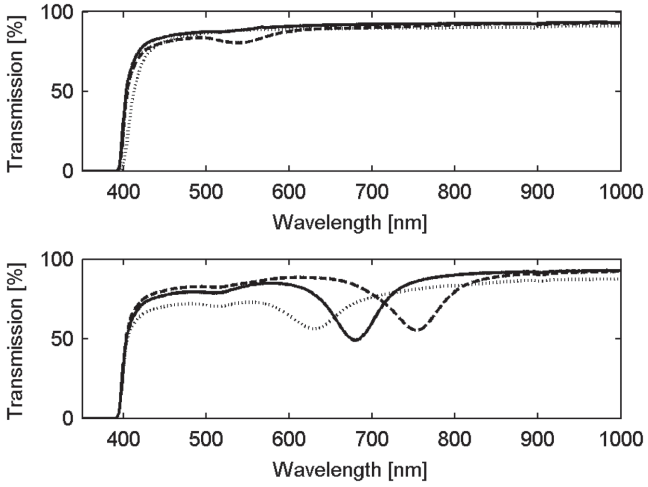

Figure 8. Transmission spectra for AuNP-chromophore **(1)** nanocomposites. The concentration of Au(0) in the glasses shown in these plots is 0.25×10^{-3} M. The upper plot shows 50×10^{-3} M of chromophore **(1)** doped MTEOS glass without gold nanoparticles (dotted line), spherical gold nanoparticles with a diameter of 23 nm (solid line) and 45 nm (dashed line). The lower plot shows 50×10^{-3} M of chromophore **(1)** doped glasses with bipyramidal gold nanoparticles with a LSP@640 nm (dotted line), a LSP@700 nm (solid line), and a LSP@770 nm (dashed line).

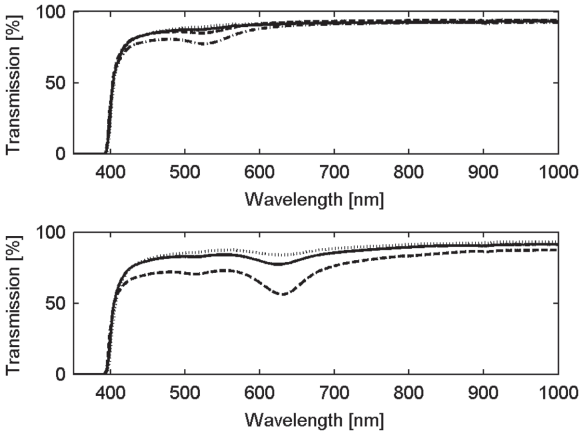

Figure 9. Transmission spectra for AuNP-chromophore **(1)** nanocomposites. The upper plot shows glasses doped with 23 nm spheres (dotted 0.06×10^{-9} M, solid 0.13×10^{-9} M, dashed 0.25×10^{-9} M, and dashed-dotted 0.5×10^{-9} M) and 50×10^{-3} M of chromophore **(1)**. The lower plot shows glasses doped with chromophore **(1)** and bipyramidal AuNP with a LSP@640 nm (dotted 0.29×10^{-9} M, solid 0.58×10^{-9} M, and dashed 1.15×10^{-9} M).

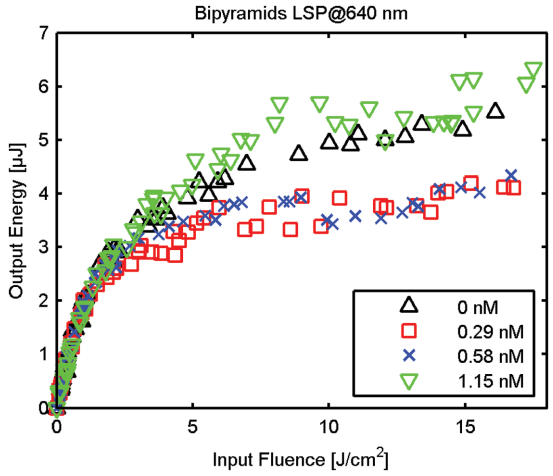

Figure 10. Nonlinear absorption curves at 600 nm for MTEOS glass doped with 50×10^{-3} M of chromophore **(1)** and bipyramidal gold nanoparticles with a LSP@640 nm. The improvement in the nonlinear absorption was largest for the glasses with the lowest concentration of gold nanoparticles.

$$\frac{\delta I}{\delta z} = \beta_0 I^2$$

Due to the square dependence of the field enhancement factor, one obtains relevant enhancement at larger distances than expected for the linear case. The two-photon field enhancement is significant and exceeds the expected 5–10 nm range of quenching dominance.[43,44] (**Figure 14**) The absorption of the surrounding medium was assumed to be low, giving $\varepsilon_m = 1.43^2$ from the measured refractive index of the glass only doped with chromophore **(1)**. The dielectric constant of gold at 600 nm was set to $\varepsilon_1 = -8.44 - 1.41i$.[57,58] At r = 100 nm, the 45 nm diameter spheres still show a relevant field enhancement of 22%.

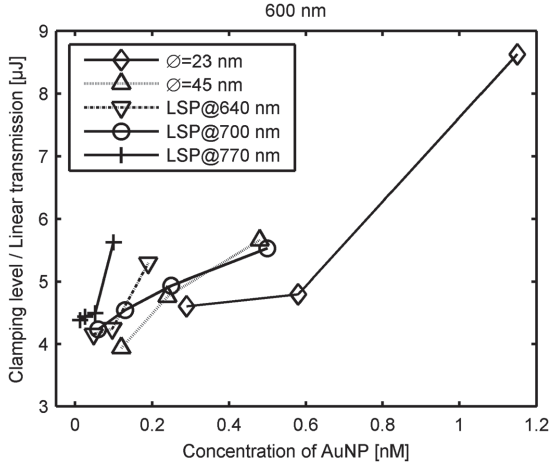

Figure 11. Comparison of the nonlinear absorption clamping level at 600 nm normalized to linear transmission versus concentration of gold nanoparticles. A pattern is found showing decreasing nonlinear absorption with increasing concentrations of gold nanoparticles.

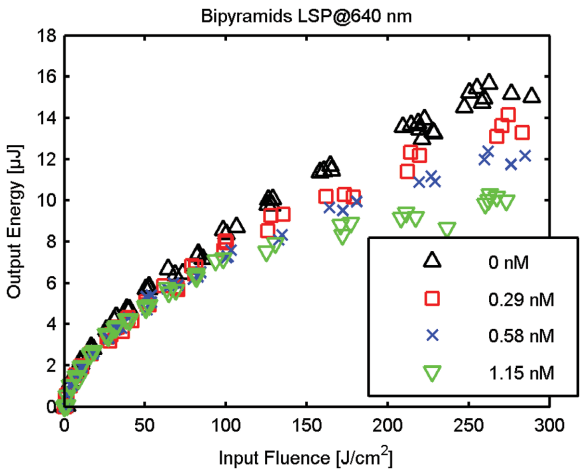

Figure 12. Nonlinear absorption curves at 532 nm for MTEOS glasses doped with 50×10^{-3} M of chromophore **(1)** and bipyramidal gold nanoparticles with an LSP@640 nm.

The population dynamics of chromophores similar to **(1)** has previously been modeled by a five level system;[59] the singlet levels of S_0, S_1, and S_N and the triplet levels T_1 and T_N. In this model, the relaxation times of S_N and T_N are assumed to be fast enough for the impacts of these levels to be negligible. The linear cross-section of S_0 to S_1 is set to 0.2 M^{-1} cm^{-1} while the linear cross-section of T_1 to T_N is set to 42000 M^{-1} cm^{-1} in accordance with spectral measurements on similar chromophores.[60] The two-photon coefficient between S_0 and S_1, β_0, is set to 290 GM.[41] The relaxation time of the triplet state is set to 42 μs,[60] while the singlet–triplet transfer time is set to 300 ps.[41]

By numerically investigating the population dynamics during a 10 J cm^{-2}, 5 ns laser pulse for different two photon field enhancements, η^2, it is possible to calculate the absorption $\alpha(\eta^2, t)$ at time t. The absorption improvement factor compared to the unenhanced case can be expressed as

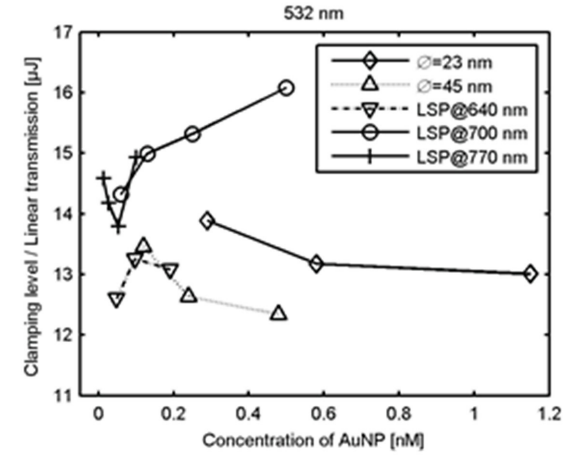

Figure 13. Comparison of the nonlinear absorption clamping level at 532 nm normalized to linear transmission versus concentration of gold nanoparticles.

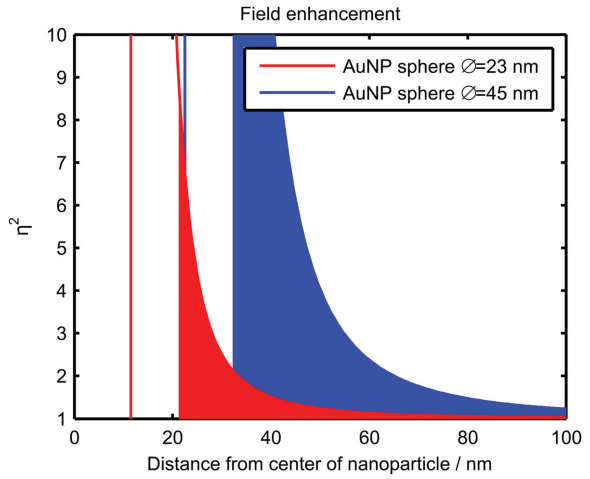

Figure 14. Estimated two-photon field enhancement factor at 600 nm excitation wavelength. The vertical lines represent the nanoparticle surface. The solid colored areas indicate distances where quenching between AuNP and chromophore is weak enough to be irrelevant.

$$\gamma(\eta^2,t)=\frac{\alpha(\eta^2,t)}{\alpha(1,t)}$$

Figure 15 shows that even long range fairly moderate two-photon field enhancements (η^2) enhance the absorption. Additionally, closer to the nanoparticles the larger effective two-photon coefficient, β, helps populate the S_1 and in turn T_1 state faster during the leading edge of the pulse. The nonlinear absorption enhancement from AuNP is, thus, the result of the nanoparticles acting as antennas funneling the field into more high intensity regions and thereby facilitating two-photon absorption. Modeling the effect of oxygen quenching by lowering the relaxation time of the triplet state to 1 µs does not impact the result noticeably. The lack of enhancement for the higher concentrations of AuNPs could be explained by linear

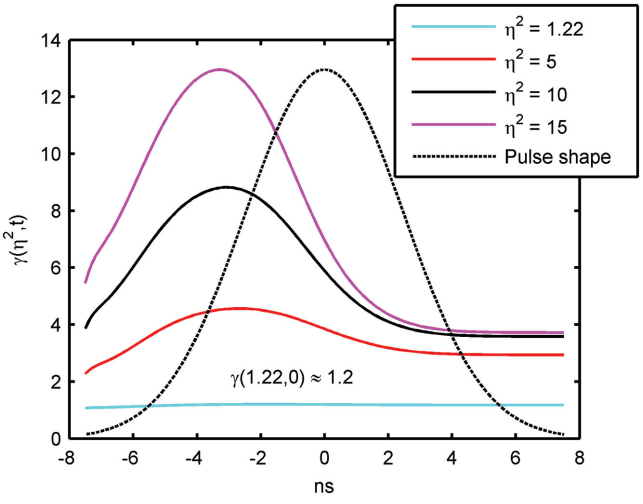

Figure 15. Improvement of absorption factor during a 5 ns laser pulse (dashed line) for different two-photon field enhancement factors (η^2) corresponding to relevant field enhancements derived from Figure 14.

absorption prior to the focal point which interferes with the nonlinear two-photon absorption. The transmittance of the AuNPs prior to the focal point (the center of the glass) can be estimated as

$$T_{\mathrm{AuNP}}=\sqrt{\frac{T}{T_0}}$$

where T is the transmittance of the glass and T_0 is the transmittance of a reference glass. The effective two-photon absorption coefficient then becomes

$$\beta=\eta^2 T_{\mathrm{AuNP}}^2\beta_0$$

By choosing T_0 to be the transmittance of the glass with the lowest AuNP concentration for each shape of AuNPs, T_{AuNP} can be estimated for each glass. For the highest AuNP concentration in each series, T_{AuNP}^2 varied between 0.97 and 0.76. Considering the low volume concentration of the AuNPs, these smaller values of T_{AuNP}^2 might ultimately have a higher impact on β than the larger values of η^2 closer to the AuNPs.

To calculate any quantitative predictions, the model has to be extended from a single point population model to a spatial model, allowing the dynamics of the populated states along the beam path. The detailed effects of η^2 relative to the position of nearby AuNPs would also have to be modeled with a more sophisticated model.

3. Conclusion

Monolithic materials containing dispersions of a chromophore and gold nanoparticles, both spheres and bipyramids, were prepared and fully characterized. They showed high homogeneity and excellent optical and mechanical qualities. Investigations of nonlinear optical properties showed that nonlinear absorption could be enhanced, but only at unexpected low concentrations of the AuNPs. The highest efficiencies, affecting the whole bulk material, were obtained for mean interparticle distances of 2–5 microns. A qualitative model showed that the nonlinear absorption enhancement resulted from local field enhancement of the two-photon absorption populating the S_1 and in turn T_1 state of chromophore **(1)**, although the local field enhancement appears to be offset by linear absorption before the focus for higher concentrations of AuNPs. The importance of excitation wavelength and AuNP concentration is also relevant for other applications where AuNPs are used. (e.g., sensors, photocatalysis, photovoltaics).

4. Experimental Section

Diethoxydimethylsilane (97%), (3-mercaptopropyl)-methyl-dimethoxysilane (95%), MTEOS (98%), (3-glycidoxypropyl)-methyl-dimethoxysilane (98%), and APTES (97%) were purchased from ABCR. HCl (37%), triethylamine (97%), ethanol (99.8%), THF (99%), diethyl ether, citric acid (99%), cetyltrimethylammonium chloride (CTAC) 25% in water, 8-hydroxyquinoline (HQL, 99%), $NaBH_4$ (99.999%), and NaOH (98%) were purchased from Sigma-Aldrich and used as received. $HAuCl_4$, $3H_2O$ (99.9%), and silver nitrate were purchased from Alfa Aesar.

Synthesis of the Gold Nanoparticles: The Au nanospheres were prepared according to previously reported procedure using the seed mediated growth method.[51]

Seeds Synthesis: The seeds were synthesized by quick injection of 400 µL of a $NaBH_4$ 50×10^{-3} M/NaOH 50×10^{-3} M mixture in a mixture of 32 mL CTAC (66×10^{-3} M), 320 µL of $HAuCl_4$ (25×10^{-3} M in water), and 296 µL of HNO_3 (0.25 M), under stirring. After 1 min, the solution was heated at 80 °C for 50 min without stirring.

Growth Solution: A mixture of 600 µL of CTAC and 200 µL of $HAuCl_4$ (25×10^{-3} M) into 19.4 mL of Milli-Q purified water was prepared. The solution was stirred for 15 min at 60 °C and 150 µL of HQL (0.4 M in THF) was added.

Spheres Growth: Finally, spherical gold nanoparticles were synthesized by adding the appropriate amount of seeds to the growth solution in order to obtain the desired size.

Synthesis of the Bipyramids: Detailed descriptions of the preparation using seed mediated process and purification of the Au bipyramids have been fully described previously.[7,17,20,51]

Seeds Synthesis: 100 µL of a cold and fresh $NaBH_4$ solution (50×10^{-3} M $NaBH_4$ and 50×10^{-3} M NaOH) was added to a solution of 4 mL $HAuCl_4$ (0.5×10^{-3} M), 4 mL CTAC (95×10^{-3} M), and 72 µL HNO_3 (250×10^{-3}M) at 20 °C, under stirring. 16 µL of citric acid (1 M) were added and the vials were closed. The vials were heated at 80–85 °C for 60 min in a water bath.

Growth of Gold Bipyramids: The growth solution was prepared by mixing 40 µL of $HAuCl_4$ (25×10^{-3} M per water) and 4 mL cetyltrimethylammonium bromide (CTAB) (47×10^{-3} M per water). 18 µL of silver nitrate solution in water (10×10^{-3} M) were added, followed by 40 µL of 8-hydroxyquinoline in ethanol (0.4 M). Respectively 300, 150, and 40 µL of the prepared gold seeds solutions were added into the growth solution under stirring for the synthesis of the bipyramids with LSPR at 640, 700, and 770 nm. The suspensions were stirred for few seconds and left at 40–45 °C for 15 min. 25 µL of 8-hydroxyquinoline in ethanol (HQL 0.4 M) were added to the mixture and left for 15 min at 40–45 °C. The suspensions were purified by centrifugation and several washing using 0.1% CTAC solution at pH = 3 (1×10^{-3} M HNO_3).

Surface Functionalization of the Au Nanoparticles Using Specific Silicone: The synthesis of the functional silicone was previously reported as well as the surface modification of the gold nanoparticles.[51] Typically, 100 µL of the functional silicone diluted in ethanol (1%) were added to 4 mL of suspension of gold nanoparticles (0.25×10^{-3} M in $[Au_0]$ for bipyramids; 0.5×10^{-3} M for spheres). The mixture was sonicated for 5 min and kept at 45 °C for 72 h. The suspension was cooled down to room temperature (RT) and 4 mL of THF was added under stirring. Addition of 0.8 mL of diethyl ether and stirring for 1 min induced a phase separation. The aqueous phase was removed and THF added to the organic phase to obtain a final suspension volume of 4 mL.

Preparation of the Monolithic Hybrid Silica Materials: The monolithic materials were prepared using an adapted procedure from previously reported method.[37,51]

In a typical procedure, the chromophore (15.3 µmoles) was dissolved in 100 µL of THF in a perfluoroalkoxy (PFA) mold. 1 g of the silica-based sol at 30% dry residues was added. The mixture was stirred and filtered using PTFE filters (porosity 0.45 µm). The desired amount of AuNP suspension in THF was added (calculated taking in consideration the final volume of the monolith after sintering). 45 µL of APTES were added and the mold was closed with stopper and left at 45 °C for 10 min. The mold was partially opened and the obtained gel was left 24 h for drying. The obtained materials were finally treated at 80 °C overnight.

Polishing of the Materials: The glasses were cut with a Buehler Isomet 1000 precision saw. They were then polished to a thickness of 1 ± 0.05 mm with a Struers polishing equipment. See the Supporting Information for pictures of the unpolished glasses.

Optical Characterization of the Materials: Refractive indices were measured using a SOPRA spectroscopic ellipsometer operating in the visible wavelengths.

UV–vis transmittance spectra were recorded either with a CARY 5G UV–vis–NIR spectrophotometer or a Perkin-Elmer UV–vis–NIR Lambda 750 spectrometer.

The nonlinear absorption measurements at 532 and 600 nm were made with the same method and on the same occasion as for the MTEOS glasses doped solely with AuNPs.[51] The glass samples were measured with varying input fluences at 532 and 600 nm with 5 ns pulse length. The 20 mm diameter top-hat beam was focused through the glass sample with a 100 mm focal length lens. The glass sample was shifted slightly in a direction perpendicular to the beam between each manually triggered laser pulse.

The area of the beam was estimated with the 10/90 knife edge method, assuming a top-hat beam. The beam diameter was measured to be 8.25 and 20.5 µm at 532 and 600 nm wavelengths, respectively.

The absorption spectroscopy, triplet ESA measurements and characterization of luminescence of samples in THF solutions were carried out as earlier described.[38,45] Here, the samples of the chromophore **(1)** with and without 45 nm diameter spherical AuNPs in different proportions were carefully bubbled with argon during measurements, or before measurements, in properly sealed 1 cm quartz cuvettes. The kinetics of the ESA was measured as earlier outlined.[38] However, for the kinetics of the excited triplet state absorption measurements, the system have been upgraded with an Applied Photophysics 5-stage photomultiplier base and a monochromator, along with an Infiniium DSO8064A oscilloscope (MS Windows based) and allowed direct recording of the transient using a synchronized 1 ms 150 W Xenon lamp as light source.

Supporting Information

Supporting Information is available from the Wiley Online Library or from the author.

Acknowledgements

The French CNRS, Swedish Armed Forces, EOARD (FA8655-12-1-2106), and AFRL are acknowledged for funding. L.-G. Heimdal is acknowledged for cutting and polishing the glass materials and Figure 5. C. Brännlund is acknowledged for taking part in the nonlinear absorption measurements.

Received: April 1, 2016
Published online: May 31, 2016

[1] F. Tam, G. P. Goodrich, B. R. Johnson, N. J. Halas, *Nano Lett.* **2007**, *7*, 496.
[2] T. K. Sau, A. L. Rogach, F. Jackel, T. A. Klar, J. Feldmann, *Adv. Mater.* **2010**, *22*, 1805.
[3] X. Meng, R. R. Grote, J. I. Dadap, N. C. Panoiu, R. M. Osgood, *Opt. Express* **2014**, *22*, 22018.
[4] S. T. Kochuveedu, D. H. Kim, *Nanoscale* **2014**, *6*, 4966.
[5] J. R. Navarro, D. Manchon, F. Lerouge, N. P. Blanchard, S. Marotte, Y. Leverrier, J. Marvel, F. Chaput, G. Micouin, A. M. Gabudean, A. Mosset, E. Cottancin, P. L. Baldeck, K. Kamada, S. Parola, *Nanotechnology* **2012**, *23*, 465602.
[6] J. R. Navarro, A. Liotta, A. C. Faure, F. Lerouge, F. Chaput, G. Micouin, P. L. Baldeck, S. Parola, *Langmuir* **2013**, *29*, 10915.
[7] J. R. Navarro, F. Lerouge, G. Micouin, C. Cepraga, A. Favier, M. T. Charreyre, N. P. Blanchard, J. Lerme, F. Chaput, M. Focsan, K. Kamada, P. L. Baldeck, S. Parola, *Nanoscale* **2014**, *6*, 5138.
[8] J. R. Navarro, F. Lerouge, C. Cepraga, G. Micouin, A. Favier, D. Chateau, M. T. Charreyre, P. H. Lanoe, C. Monnereau, F. Chaput, S. Marotte, Y. Leverrier, J. Marvel, K. Kamada, C. Andraud, P. L. Baldeck, S. Parola, *Biomaterials* **2013**, *34*, 8344.
[9] X. L. Liu, J. H. Wang, S. Liang, D. J. Yang, F. Nan, S. J. Ding, L. Zhou, Z. H. Hao, Q. Q. Wang, *J. Phys. Chem. C* **2014**, *118*, 9659.

[10] S. Zaiba, F. Lerouge, A. M. Gabudean, M. Focsan, J. Lerme, T. Gallavardin, O. Maury, C. Andraud, S. Parola, P. L. Baldeck, *Nano Lett.* **2011**, *11*, 2043.
[11] I. Cohanoschi, F. E. Hernandez, *J. Phys. Chem. B* **2005**, *109*, 14506.
[12] N. S. Abadeer, M. R. Brennan, W. L. Wilson, C. J. Murphy, *ACS Nano* **2014**, *8*, 8392.
[13] S. T. Sivapalan, J. H. Vella, T. K. Yang, M. J. Dalton, R. N. Swiger, J. E. Haley, T. M. Cooper, A. M. Urbas, L. S. Tan, C. J. Murphy, *Langmuir* **2012**, *28*, 9147.
[14] T. Zhao, K. Yu, L. Li, T. Zhang, Z. Guan, N. Gao, P. Yuan, S. Li, S. Q. Yao, Q. H. Xu, G. Q. Xu, *ACS Appl. Mater. Interfaces* **2014**, *6*, 2700.
[15] W. Ni, Z. Yang, H. Chen, L. Li, J. Wang, *J. Am. Chem. Soc.* **2008**, *130*, 6692.
[16] M. Grzelczak, J. Perez-Juste, P. Mulvaney, L. M. Liz-Marzan, *Chem. Soc. Rev.* **2008**, *37*, 1783.
[17] J. R. Navarro, D. Manchon, F. Lerouge, E. Cottancin, J. Lerme, C. Bonnet, F. Chaput, A. Mosset, M. Pellarin, S. Parola, *Nanotechnology* **2012**, *23*, 145707.
[18] M. R. Langille, M. L. Personick, J. Zhang, C. A. Mirkin, *J. Am. Chem. Soc.* **2012**, *134*, 14542.
[19] X. Kou, W. Ni, C. K. Tsung, K. Chan, H. Q. Lin, G. D. Stucky, J. Wang, *Small* **2007**, *3*, 2103.
[20] D. Chateau, A. Liotta, F. Vadcard, J. R. Navarro, F. Chaput, J. Lerme, F. Lerouge, S. Parola, *Nanoscale* **2015**, *7*, 1934.
[21] E. Hutter, J. H. Fendler, *Adv. Mater.* **2004**, *16*, 1685.
[22] S. Eustis, M. A. El-Sayed, *Chem. Soc. Rev.* **2006**, *35*, 209.
[23] Q. Gan, F. J. Bartoli, Z. H. Kafafi, *Adv. Mater.* **2013**, *25*, 2385.
[24] M. Notarianni, K. Vernon, A. Chou, J. Liu, N. Motta, *Adv. Device Mater.* **2015**, *1*, 27.
[25] S. Sandén, K. Akitsu, B. Törngren, A. Ylinen, J.-H. Smått, T. Kubo, M. Matsumura, N. Otani, H. Segawa, R. Österbacka, *J. Phys. Chem. C* **2015**, *119*, 5570.
[26] C.-S. Chang, L. J. Rothberg, *Chem. Mater.* **2015**, *27*, 3211.
[27] T.-M. Chien, P. Pavaskar, W. H. Hung, S. Cronin, S.-H. Chiu, S.-N. Lai, *J. Nanomater.* **2015**, *2015*, 1.
[28] J. Choi, S.-H. Ji, C.-S. Choi, J.-W. Oh, F. S. Kim, N. Kim, *Opt. Lett.* **2014**, *39*, 4571.
[29] W. Park, D. Lu, S. Ahn, *Chem. Soc. Rev.* **2015**, *44*, 2940.
[30] S. Khatua, P. Manna, W. S. Chang, A. Tcherniak, E. Friedlander, E. R. Zubarev, S. Link, *J. Phys. Chem. C* **2010**, *114*, 7251.
[31] I. Suleimanov, J. Sanchez Costa, G. Molnar, L. Salmon, A. Bousseksou, *Chem. Commun.* **2014**, *50*, 13015.
[32] A. Wang, Y. Fang, L. Long, Y. Song, W. Yu, W. Zhao, M. P. Cifuentes, M. G. Humphrey, C. Zhang, *Chem. Eur. J.* **2013**, *19*, 14159.
[33] S. Dengler, C. Hege, B. Eberle, *Proc. SPIE* **2014**, *9253*, 9253171.
[34] M. P. Joshi, J. Swiatkiewicz, F. Xu, P. N. Prasad, B. A. Reinhardt, R. Kannan, *Opt. Lett.* **1998**, *23*, 1742.
[35] P. Sudheesh, N. K. S. Narendran, K. Chandrasekharan, *Opt. Mater.* **2013**, *36*, 304.
[36] D. Riehl, N. Izard, L. Vivien, E. Anglaret, E. Doris, C. Ménard, C. Mioskowski, L. Porrès, O. Mongin, M. Charlot, M. Blanchard-Desce, R. Anémian, J.-C. Mulatier, C. Barsu, C. Andraud, *Proc. SPIE* **2003**, *5211*, 124.
[37] D. Chateau, F. Chaput, C. Lopes, M. Lindgren, C. Brannlund, J. Ohgren, N. Djourelov, P. Nedelec, C. Desroches, B. Eliasson, T. Kindahl, F. Lerouge, C. Andraud, S. Parola, *ACS Appl. Mater. Interfaces* **2012**, *4*, 2369.
[38] E. Glimsdal, I. Dragland, M. Carlsson, B. Eliasson, T. B. Melø, M. Lindgren, *J. Phys. Chem. A* **2009**, *113*, 3311.
[39] R. Westlund, E. Malmström, C. Lopes, J. Öhgren, T. Rodgers, Y. Saito, S. Kawata, E. Glimsdal, M. Lindgren, *Adv. Funct. Mater.* **2008**, *18*, 1939.
[40] C. Liao, A. H. Shelton, K. Y. Kim, K. S. Schanze, *ACS Appl. Mater. Interfaces* **2011**, *3*, 3225.
[41] M. G. Vivas, L. De Boni, T. M. Cooper, C. R. Mendonca, *J. Phys. Chem. A* **2014**, *118*, 5608.
[42] J. Zhang, T. He, C. Wang, X. Zhang, Y. Zeng, *Opt. Laser Technol.* **2011**, *43*, 974.
[43] P. Anger, P. Bharadwaj, L. Novotny, *Phys. Rev. Lett.* **2006**, *96*, 113002.
[44] M. Thomas, J.-J. Greffet, R. Carminati, J. R. Arias-Gonzalez, *Appl. Phys. Lett.* **2004**, *85*, 3863.
[45] M. Lindgren, B. Minaev, E. Glimsdal, R. Vestberg, R. Westlund, E. Malmström, *J. Lumin.* **2007**, *124*, 302.
[46] P. Lind, D. Boström, M. Carlsson, A. Eriksson, E. Glimsdal, M. Lindgren, B. Eliasson, *J. Phys. Chem. A* **2007**, *111*, 1598.
[47] C. Sanchez, B. Lebeau, F. Chaput, J. P. Boilot, *Adv. Mater.* **2003**, *15*, 1969.
[48] C. Desroches, C. Lopes, V. Kessler, S. Parola, *Dalton Trans.* **2003**, 2085.
[49] R. Zieba, C. Desroches, F. Chaput, M. Carlsson, B. Eliasson, C. Lopes, M. Lindgren, S. Parola, *Adv. Funct. Mater.* **2009**, *19*, 235.
[50] D. Château, Q. Bellier, F. Chaput, P. Feneyrou, G. Berginc, O. Maury, C. Andraud, S. Parola, *J. Mater. Chem. C* **2014**, *2*, 5105.
[51] H. Lundén, A. Liotta, D. Chateau, F. Lerouge, F. Chaput, S. Parola, C. Brännlund, Z. Ghadyani, M. Kildemo, M. Lindgren, C. Lopes, *J. Mater. Chem. C* **2015**, *3*, 1026.
[52] D. Chateau, *Ph.D. Thesis, Ecole Normale Supérieure de Lyon (France)* **2013**.
[53] J. Zhang, L. Zhang, *Adv. Opt. Photonics* **2012**, *4*, 157.
[54] N. J. Halas, S. Lal, W. Chang, S. Link, P. Nordlander, *Chem. Rev.* **2011**, *111*, 3913.
[55] S. Fischer, F. Hallermann, T. Eichelkraut, G. V. Plessen, K. W. Krämer, D. Biner, H. Steinkemper, M. Hermle, J. C. Goldschmidt, *Opt. Express* **2012**, *20*, 271.
[56] K. Tanabe, *J. Phys. Chem. C* **2008**, *112*, 15721.
[57] A. D. Rakić, A. B. Djurišic, J. M. Elazar, M. L. Majewski, *Appl. Opt.* **1998**, *37*, 5271.
[58] M. N. Polyanskiy, *Refractive Index Database*, http://refractiveindex.info (accessed: February **2016**).
[59] E. Glimsdal, *Ph.D. Thesis*, Norwegian University of Science and Technology (Norway), **2009**.
[60] J. E. Rogers, T. M. Cooper, P. A. Fleitz, D. J. Glass, D. G. McLean, *J. Phys. Chem. A* **2002**, *106*, 10108.